A 3D Foot-Ground Model using Disk Contacts

M.Millard and A.Kecskeméthy

Abstract A foot contact model is an important component of any forward-dynamic human gait simulation. This work presents a preliminary experimental validation of a three-dimensional (3D) foot contact model that represents the heel and forefoot using a pair of contact disks. The disk elements are well-suited to modeling the foot because they are computationally efficient and are mechanically stable when flat on the ground. We evaluated the foot model by comparing its ankle position to the subject's ankle position (measured using skin-mounted reflective markers and infrared cameras) when both feet developed the same ground reaction force (GRF) and center-of-pressure (COP) profiles (measured using a force plate). We used this novel approach because the experimental GRF and COP measurements are accurate, but the kinematic data is usually corrupted with 1 cm of skin-movement error at the foot. The results indicate that the disk-based foot model is an accurate representation of the subject's barefoot except during toe-off, and when the COP is on the extreme medial boundaries of the foot. The experimental data and foot model presented in this work is provided as supplementary material online.

1 Introduction

Human motion prediction *in-silico* is of great interest to many research communities because of its potential to improve our understanding of healthy and pathological locomotion. During normal bipedal locomotion feet are the only contacts that interact with the ground. A validated model of the human foot is thus a pre-requisite for a computed prediction of human gait.

M.Millard
Universität of Duisburg-Essen, Duisburg, Germany. e-mail: matthew.millard@uni-due.de

A.Kecskeméthy
Universität of Duisburg-Essen, Duisburg, Germany. e-mail: andres.kecskemethy@uni-due.de

A predictive gait simulation requires a foot model that can simultaneously reproduce the kinematics, ground reaction forces (GRF) and center-of-pressure (COP) profile of a human foot. In addition, a 3D foot contact model must be as stable as a human foot, so that the ankle does not roll unrealistically during simulation. Although the foot can be modeled using realistic geometry [17], this is computationally expensive. Instead, most foot contact models use fast, but simplified contact-pairs to represent the foot: point-plane [16, 15, 1, 5, 13, 18], circle-plane (2D) [12], sphere-plane [14, 3], and disk-plane (3D) [9]. Here we focus on the disk-based 3D foot contact model [9] because the disk contact approximates the round shape of the foot pads, is mechanically stable, and is computationally efficient.

Though the foot has been modeled using a variety of approaches, relatively few foot-ground contact models have been tested against experimental data [5, 12, 9]. Conceptually a foot contact model transforms a kinematic state into a wrench applied at the ankle, and vice-versa (though the mapping from wrench to kinematic state is not unique). A good validation method matches one side of this transformation to experimental data, and then evaluates the model against experimental data using the other side of the transformation.

The development of well-posed, well-behaved foot contact validation methods is an area of active research. Skin-movement artifact precludes using one-to-one experimental kinematics as input to the foot contact model and then evaluating it by comparing simulated GRF and COP profiles to experimental data [12]: the 1 cm of skin movement error at the foot [7] is comparable to the expected heel [4] and metatarsal pad compressions [2]. Numerical instability precludes applying the observed wrench to the model's ankle, forward integrating, and then evaluating the model by comparing simulated foot kinematics to experimental kinematics [5]: applying large forces to a body of low mass results in a simulation that is very sensitive to initial conditions and experimental error. This approach can be vastly improved by ignoring the dynamics of the foot, solving for a position of static equilibrium, and comparing the resulting foot orientation to experimental data [9] though the resulting root-finding problem is not easily solved. In this paper we present a novel control system which drives the ankle of the foot model to a trajectory that reproduces the accurately measured GRF and COP profiles. We evaluate the model by comparing its ankle kinematics to experimental observations: distance errors of 1 cm [7] or less are acceptable, since this amount of skin-movement error is present in motion capture data.

The experimental tasks that are used to validate the foot contact model are just as important as the validation methods. Although walking data is commonly used to evaluate foot contact models [5, 12, 9], additional motions should be used because the kinematics of the foot and its COP profile during walking are mostly in the sagittal plane. We have recorded a novel trial where the subject moves the COP of their barefoot in the pattern of a growing spiral which eventually traces the outer edge of their foot. The spiraling-COP task allows the foot model to be tested against motions in both the sagittal and frontal planes, providing a more comprehensive evaluation of the foot-ground contact model.

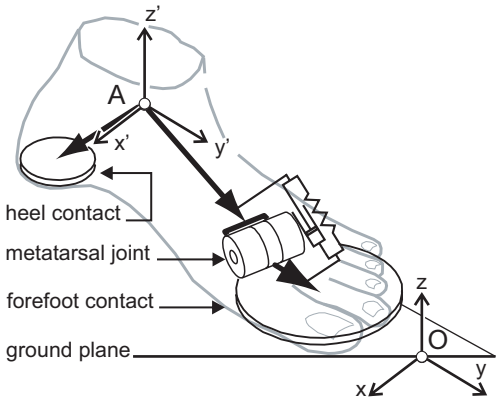

Fig. 1 The foot interacts with the ground plane through two disk contacts. The heel disk is rigidly attached the ankle frame (frame A). A revolute metatarsal joint allows the fore-foot disk to rotate with respect to the heel disk. A spring-damper across the metatarsal joint applies a torque to the ankle frame. The left foot is shown because the subject's left foot was instrumented.

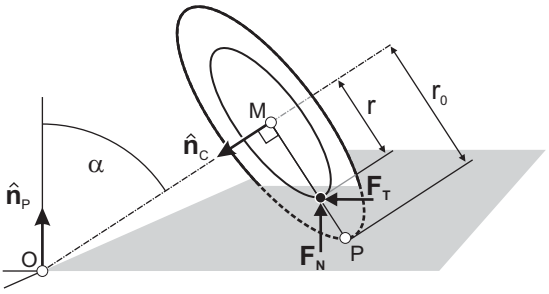

Fig. 2 The contact point of the disk model [10], shown in black, is smoothly brought to the center of the disk as it flattens (as $\alpha \to 0$). The smooth transition makes the contact kinematics of the disk similar to those of an infinitely thin rounded surface. The rounded appearance of the disk lends itself to simulating human foot pads, which have a flat bottom and rounded edges.

2 Foot Model

The 3D foot contact model is composed of a hind foot, and a forefoot body joined together by a revolute joint. The axis of this joint has been rotated 22° about the $\hat{z}'$ axis to match the raked alignment of the subject's metatarsal joints. The musculature of the toes is represented with a nonlinear spring-damper element in parallel with the revolute joint. The heel contact is represented by a disk [10] attached to the hind foot, while the metatarsal and toe contacts are represented by a single disk attached to the forefoot body (Fig. 1).

The disk interacts with the ground plane through a point contact [10]. The point contact lies in the direction

$$ {}_M\hat{\mathbf{u}}_P = \hat{\mathbf{n}}_C \times (\hat{\mathbf{n}}_C \times \hat{\mathbf{n}}_P) \tag{1} $$

which points from the center of the disk to point P, the lowest point on the disk edge. This direction vector is computed using the surface normal vector $\hat{\mathbf{n}}_C$ and the disk normal vector $\hat{\mathbf{n}}_P$. The contact point is located along ${}_M\hat{\mathbf{u}}_P$ at a distance of

$$r = r_0(1 - e^{-C\sin\alpha}) \tag{2}$$

from the center of the disk, where α is the angle between the surface and disk normal vectors. An exponential function makes the disk appear rounded by smoothly blending r from 0, when the disk is flat on the ground ($\alpha = 0$), to approach the disk radius r_0, when the disk is perpendicular to the ground plane ($\alpha = \frac{\pi}{2}$). The parameter C is used to control how rounded the disk appears. Low values of C will make the disk edges appear more rounded, while high values of C will make the disk appear sharper.

Once the point contact location has been computed, the state of the disk contact is used to calculate the penetration depth, x_N, and velocity, v_N, of the point contact into the surface. Here we use a Hunt-Crossley contact model [8] to compute the normal force magnitude

$$F_N^* = kx_N^P(1 + dv_N) \tag{3}$$

with the condition that only positive normal contact forces are permitted, i.e.

$$\mathbf{F}_N = \begin{cases} F_N^* \cdot \hat{\mathbf{n}}_P & \text{if } F_N^* > 0 \\ 0 & \text{otherwise} \end{cases} \tag{4}$$

. A Coulomb friction model is used to compute tangential contact forces

$$\mathbf{F}_T = -\mu(|\mathbf{v}_T|_2)F_N\hat{\mathbf{v}}_T \tag{5}$$

using the tangential velocity $\mathbf{v}_T$ between the point contact and the surface. The coefficient of friction μ is smoothly interpolated (using a cubic spline) to make the system equations less stiff. We compute the tangential velocity direction, $\hat{\mathbf{v}}_T$, using the numerically stable method described in Eqn. 20 of Gonthier et al. [6].

3 Methods

We evaluated the foot contact model using experimental foot kinematic and kinetic data collected during a conventional barefoot walking task, and a novel task designed to move the COP over the entire bottom surface of the foot in the pattern of a growing spiral. The COP-spiral began with COP rotations about the subject's midfoot, and grew over 5 rotations to the outside of the subject's foot while under a load of $\approx 3/4$ bodyweight (the subject held onto a support to maintain balance during this task). Foot kinematics were measured using infrared cameras and skin-mounted reflective markers, while ground reaction forces and moments were measured using a floor-mounted force plate.

To evaluate the foot contact model we computed the Euclidean distance between the subject's ankle position $\tilde{\mathbf{r}}_A(t)$ and the model's ankle position $\mathbf{r}_A(t)$ (Fig.1)

$$\varepsilon(t) = ||\tilde{\mathbf{r}}_A(t) - \mathbf{r}_A(t)|| \tag{6}$$

when both feet generated the same GRF and COP profiles (experimental quantities indicated using the tilde symbol). In the context of this error measure, an excellent foot contact model will be able to remain within a skin-movement distance ($\varepsilon \leq 1\,cm$ [7]) of the subject's ankle while accurately reproducing the observed GRF and COP profiles. We used this novel evaluation method because it allows the foot model to be evaluated accurately in the presence of skin-movement error.

A control system and forward-simulation was used to compute the path of the foot model that reproduced the experimental GRF and COP profiles. The control system consists of three parts: a feed-forward wrench computed from the experimental data $\tilde{\mathbf{W}}$, a kinematic feedback proportional-derivative (PD) tracking controller ($[\mathbf{P}]\mathbf{q}_e + [\mathbf{D}]\dot{\mathbf{q}}_e$), a force feedback controller $[\mathbf{E}]\mathbf{W}_e$, and a damping wrench $[\mathbf{V}]\dot{\mathbf{q}}$:

$$\mathbf{W}_u = \tilde{\mathbf{W}} + (1-s)\,C_Q\,([\mathbf{P}]\mathbf{q}_e + [\mathbf{D}]\dot{\mathbf{q}}_e) + s\,C_W\,[\mathbf{E}]\mathbf{W}_e + s\,C_V\,[\mathbf{V}]\dot{\mathbf{q}} \tag{7}$$

. Here a subscript e, as in q_e of Eqn.7, is used to indicate an error, defined as the difference between an experimental observation and the corresponding value in the simulation. All of the gain matrices in Eqn. 7 are diagonal, and have been tuned by hand. The tracking, force-feedback, and damping control terms in Eqn.7 are scaled by task dependent scalar gain variables C_Q, C_W, and C_V respectively. These gains are tuned so that the model's GRF and COP profiles quickly and smoothly converge to the experimentally measured profiles during the walking and spiral tasks. A blending variable

$$s = \frac{\tilde{F}_N(t)}{\max(\tilde{F}_N(t))} \tag{8}$$

is used to ensure the kinematic tracking controller dominates when contact forces are low, and the force feedback controller dominates when contact forces are high. The results of a forward simulation are used to compute $\varepsilon(t)$ in Eqn. 6, the distance between the subject's ankle and the model's ankle.

The parameters of the foot model were tuned using the distance error ε to guide changes. The geometric parameters of the foot model were initially matched as closely as possible to the subject's foot using manual measurements. The stiffness of the contact disks were set so that the heel and metatarsal pads compress by approximately 50% of their unloaded thickness during stance [4]. For this subject, a 50% compression of the heel pad amounts to 11.4 mm (22.8 mm thick), and 6.7 mm (13.2 mm thick) for the 2^{nd} metatarsal pad. The thickness of the subject's foot pads were measured previously using an ultrasound scanner. The stiffness and damping of the toe joint was initially manually set. A combination of derivative-free optimization and hand tuning was used to adjust the geometry of the foot and the stiffness of the toe joint to find a single set of parameters that fit the experimental data taken from the walking and spiraling-COP tasks.

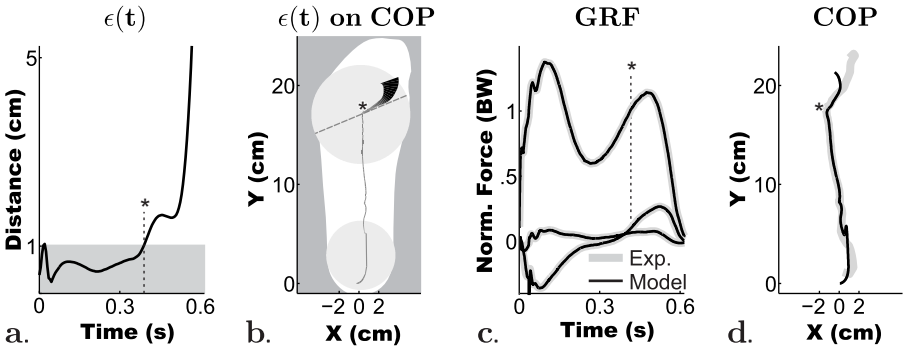

Fig. 3 Panel a. illustrates the distance error, $\varepsilon(t)$, between the model's ankle and the subject's ankle during the walking experiment. The error exceeds 1cm at $t = 0.39s$, which is marked with an '*'. Panel b. illustrates the COP (as seen from above) on the surface of the model's foot, using a line that becomes thicker and darker as the distance error, $\varepsilon(t)$, increases. The dashed line shows the axis of rotation of the metatarsal joint (n.b. left foot is shown). To provide context, the outside of the subject's foot is shown in white, and the disk contacts are shown in light gray. Panels c. and d. illustrate the GRF and COP profiles of the model (black line) and the experiment (grey line).

4 Results and Discussion

The walking trial shows that the model foot is indistinguishable from the subject's foot until toe-off. The distance error, ε, between the model's ankle and the subject's ankle is less than the experimental skin-stretch error of 1 cm [7] until $t = 0.39$ s (Panel a. of Fig.3). An association between error and the foot model is made in Panel b. of Fig.3 by plotting the COP projected on the model foot, using a line that becomes thicker and darker as the distance error, ε, increases. The thickest and darkest lines of the COP error plot (Panel b. of Fig. 3) show that the distance error is small until the COP extends past the metatarsal joint (Panel b. of Fig. 3), the equivalent location of the subject's big toe. The control system drives the model to accurately track the experimental GRF and COP profiles with little error, except during heel contact and toe-off (Panels c. and d. of Fig.3). The COP error that occurs during initial heel contact ($t = 0$ s) is caused by a shape mismatch between the heel disk and the subject's heel in the initial pose. Due to this shape mismatch we could not simultaneously collocate both the ankle and the COP at the start of the stance phase. We chose to match the position of the ankle, introducing an error in the COP profile, so that the two ankles would continue to align as the foot rotated and flattened on the ground plane. The COP error at toe-off occurs because the contact disk does not extend far enough to cover the contact patch of the big toe.

The spiraling-COP trial results show that the model foot closely tracks the experimental data for the first 3 COP rotations (4.6 s). The error steadily accumulates during the entire trial, we suspect, due to small differences in the shape of the model's foot and the subject's foot. The distance error, ε, can be associated with a location on the foot model in Panel b. of Fig.3 by plotting the COP projected onto the surface

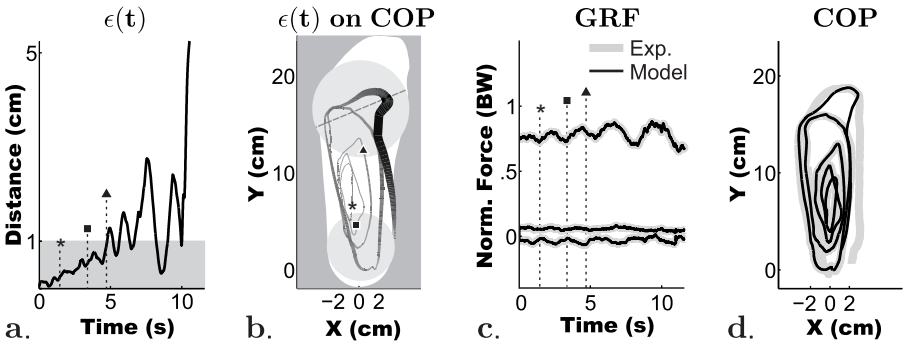

Fig. 4 Panel a. illustrates the distance error, $\varepsilon(t)$, between the model ankle and the human ankle during the spiraling-COP task. The first 3 rotations are marked using '*','■', and '▲' symbols. Panel b. illustrates the COP (as seen from above) on the surface of the model's foot, using a line that becomes thicker and darker as the distance error, $\varepsilon(t)$, increases. The dashed line shows the axis of rotation of the metatarsal joint of the left foot. To provide context, the outside of the subject's foot is shown in white, and the disk contacts are shown in light gray. Panels c. and d. illustrate the GRF and COP profiles from the model (black line) and the experiment (grey line).

of the model foot using a line that becomes thicker and darker as the distance error ε increases. At the beginning of the trial, the COP-error line is light and thin, but steadily grows with each subsequent rotation (Panel b. of Fig.4). During the final rotation, both the distance error ε and the COP tracking error become large as the COP traverses the subject's toe, and proceeds down the medial side of the subject's left foot. The COP was on the extreme edge of the subject's foot, which was everted by 21° (relative to the ground plane), during this final movement.

The high level of agreement between the model and experimental data during these two different tasks is very encouraging. In both tasks, the model matches the data within experimental error when the COP is on the heel, or is between the heel and metatarsal joint. It is only when the COP is beyond the metatarsal joint, or when the foot is everted by 21° (about the ground plane), that the model's ankle kinematics differ substantially from the experimental data. The error between the model and the experimental data during the final loop of the spiral task is acceptable for most simulations since it required an extreme tilt of 21°. The close agreement during the first 3 rotations of the spiraling-COP task suggests that the model's heel and mid-foot is as resistant to ankle rolling as the subject's foot. Further efforts will concentrate on improving the fidelity of the toe, and characterizing the model's stability. The data and software required to reproduce these results are available online [11].

Acknowledgements The authors gratefully acknowledge Dr. Dominik Raab for his generous assistance with the data collection. This work was co-funded by the German federal state North Rhine Westphalia (NRW) and the European Union (European Regional Development Fund: Investing In Your Future).

References

1. M. Ackermann and A. J. van den Bogert. Optimality principles for model-based prediction of human gait. *J Biomech*, 43(6):1055 – 1060, 2010.
2. P. Cavanagh. Plantar soft tissue thickness during ground contact in walking. *J Biomech*, 32:623–628, 1999.
3. J. Cuadrado, R. Pàmies-Vilà, U. Lugrís, and J. F. Alonso. A force-based approach for joint-efforts estimation during the double support phase of gait. In *Procedia IUTAM*, volume 2, 2011. Waterloo,Canada.
4. A. Gefen, M. Megido-Ravid, and Y. Itzchak. In vivo biomechanical behavior of the human heel pad during the stance phase of gait. *J Biomech*, 34:1661–1665, 2001.
5. L. Gilchrist and D. Winter. A two-part viscoelastic foot model for use in gait simulations. *J Biomech*, 29(6):795–798, 1996.
6. Y. Gonthier, J. McPhee, C. Lange, and J. Piedboeuf. A regularized contact model with asymmetric damping and dwell-time dependent friction. *MULTIBODY SYST DYN*, 11:209–233, 2004.
7. J. P. Holden, J. A. Orsini, K. L. Siegel, T. M. Kepple, L. H. Gerber, and S. J. Stanhope. Surface movement errors in shank kinematics and knee kinetics during gait. *Gait Posture*, 5(3):217–227, 1997.
8. K. Hunt and F. Crossley. Coefficient of restitution interpreted as damping in vibroimpact. *J APPL MECH-T ASME*, 42(E):440445, 1975.
9. A. Kecskeméthy. Integrating efficient kinematics in biomechanics of human motions. In *Procedia IUTAM*, volume 2, 2011. Waterloo,Canada.
10. A. Kecskeméthy, C. Lange, and G. Grabner. A geometric model for cylinder-cylinder impact with application to vertebrae motion simulation. In J. Lenarčic and M. Stanišić, editors, *Advances in Robot Kinematics*, pages 345–354. Springer Netherlands, 2000.
11. M. Millard and A. Kecskeméthy. Supplimentary material for: A 3d foot-ground model using disk contacts, 2013. www.uni-due.de/mechanikb/forschung/Publikationen.php#2013.
12. M. Millard, J. McPhee, and E. Kubica. Multi-step forward dynamic gait simulation. In C. Bottasso, editor, *Multibody Dynamics: Computational Methods and Applications*, pages 25–43. Springer, 2009.
13. R. R. Neptune, I. C. Wright, and A. J. van den Bogert. A method for numerical simulation of single limb ground contact events: Application to heel-toe running. *COMPUT METHOD BIOMEC*, 3:321–334, 2000.
14. R. Pàmies-Vilà, J. Font-Llagunes, U. Lugrís, and J. Cuadrado. Two approaches to estimate foot-ground contact model parameters using opitmization techniques. In *IMSD*, 2012. Stuttgart, Germany.
15. M. Peasgood, E. Kubica, and J. McPhee. Stabilization of a dynamic walking gait simulation. *J COMPUT NONLIN DYN*, 2:65–72, 2007.
16. S. Scott and D. A. Winter. Biomechanical model of the human foot: kinematics and kinetics during the stance phase of walking. *J Biomech*, 26:1091–1104, 1998.
17. A. Seth, M. Sherman, J. A. Reinbolt, and S. L. Delp. Opensim: a musculoskeletal modeling and simulation framework for *in silico* investigations and exchange. In *Procedia IUTAM*, volume 2, 2011. Waterloo,Canada.
18. C. Wilson, M. A. King, and M. R. Yeadon. Determination of subject-specific model parameters for visco-elastic elements. *J Biomech*, 39(10):1883–1890, 2006.